31st Annual International Conference of the IEEE EMBS
Minneapolis, Minnesota, USA, September 2-6, 2009

Gradient Vector Flow based Active Shape Model for Lung Field Segmentation in Chest Radiographs

Tao Xu, Mrinal Mandal, Richard Long and Anup Basu

Abstract—**Accurate lung field segmentation is crucial to computer-aided diagnosis (CAD) of lung diseases such as lung cancer and tuberculosis (TB). In this paper, we propose a modified gradient vector flow based active shape model (GVF-ASM) for lung field extraction from chest radiographs. Experimental results show that the proposed technique provides around 3-5% improvement over the ASM techniques.**

I. Introduction

ALTHOUGH thoracic imaging research has been moving towards new techniques such as CT or MRI over the past decade, conventional chest radiograph (CXR) is still the most common type of radiological procedure, making up at least one third of all exams in a typical radiology department [1]. Lung field segmentation plays an important role in quantification of tissue volumes, lung disease diagnosis, localization of pathology, study of anatomical structure and so on. However, extracting an accurate lung field from a chest radiograph is extremely challenging due to the high variability of lung shapes and the variation in image quality.

Previous efforts made for lung field segmentation can be broadly categorized into two main groups: low level and high level methods. Low level processing refers to pixel and/or region intensity based segmentation methods, such as thresholding [2], edge detection and linking [3], and hybrid of edge enhancement and thresholding method [4]. These techniques are usually automatic but encounter problems in case of variability among images. On the other hand, high level processing tries to utilize prior knowledge of generic thoracic images including global and/or local features. For example, deformable model incorporating edge information called Active Contour Model (also known as Snake) [5], and deformable model incorporating prior knowledge called Active Shape Model (ASM) [6] have been shown to be effective for segmenting lung field.

Snake is a curve evolution method based on the balance of external and internal forces or energies [7]. The internal force is a parametric model which ensures the curve stretchable and bendable, and the external force drives the curve to desired image features, such as edges, lines and terminations. Since the Snake's internal force only keeps the shape smooth and is sensitive to parameters selection, Cootes et al [8] proposed the ASM method which applied a statistical shape model incorporating the prior knowledge of the object for more accurate segmentation. However, both typical ASM and Snake use local image features for curve evolution. Without global regulation, the performances of these local schemes rely heavily on good initialization. If the initialization is not done properly, the control points may get trapped in a local optimum during search. To increase the robustness, Xu et al [9] proposed a Gradient Vector Flow-based Snake (GVF-Snake) by diffusing the gradient vectors of the image into a global field and used this field as Snake's external force to guide points evolution. Furthermore, Yuan et al [10] incorporated the GVF into ASM method for image segmentation. However, its points evolution equation is linear to the GVF and may not be efficient for segmentation.

In this paper, we propose a modified GVF-ASM method using a nonlinear function of the global GVF field for shape model fitting. The points evolution is regulated by both the direction and magnitude of the global GVF field. Algorithms are applied to 50 (normal and abnormal) chest radiographs and the segmentation results are compared with the ground truth contours specified by an expert.

The rest of this paper is organized as follows: Section II provides brief related background work on the ASM-based segmentation methods. In Section III, our method is described in detail, followed by Section IV which shows the experimental results. Conclusions are discussed in Section V.

II. Review of Related Work

This section briefly reviews the ASM segmentation scheme which was first proposed by Cootes et al in [8] and later refined by many researchers [6] [10]. The general layout of the ASM-based segmentation methods contains two parts: 1) a Point Distribution Model (PDM) generated in the training stage; 2) an iterated algorithm used for fitting the model by minimizing some cost function in the test stage.

A. PDM Generation

The kernel part of the ASM method is the PDM, which usually includes a shape model and a gray level appearance model (or profile model) based on the statistical analysis of training images.

Shape Model: A deformable shape model is computed by M shapes from the training images. Assume that each shape is

Manuscript received on April 7th, 2009.

Tao Xu and Mrinal Mandal are with the Dept. of Electrical and Computer Engineering, University of Alberta , Edmonton, AB, T6G 2V4 CA (e-mail: tx1@ualberta.ca, mandal@ece.ualberta.ca). Richard Long is with the Dept. of Medicine, Faculty of Medicine and Dentistry, University of Alberta, Edmonton, AB T6G 2R7 CA (e-mail: richard.long@ualberta.ca). Contact author: Anup Basu is with the Dept. of Computing Science, University of Alberta, Edmonton, AB T6G 2H1 CA (e-mail: anup@cs.ualberta.ca).

represented with N points annotated by a human observer, the i^{th} contour C^i in the training images is a set of N points:

$$C^i = \left\{(x_1^i, y_1^i), (x_2^i, y_2^i), ...(x_N^i, y_N^i)\right\}, i = 1, 2, ...M. \quad (1)$$

By performing a Principal Component Analysis (PCA), any shape in the training set can be approximated by:

$$C \approx \bar{C} + Pb \quad (2)$$

where $\bar{C}$ denotes the mean shape of the training set, $P=[p_1,p_2,...p_l]$ with size of $2N \times l$ is the matrix of the first l eigenvectors, and $b=[b_1,b_2,...b_l]^T$ is a vector of weights that defines the shape parameters. By allowing a variation range, this method ensures the gross similarity among shapes.

Profile Model: PCA is applied to characterize the gray level variation of each control point in the shape model, i.e.:

$$z = \bar{z} + P_z b_z \quad (3)$$

where $\bar{z}$ denotes the mean gradient profile along each control point's normal direction, P_z is a matrix consisting of significant modes of gray level variations, and b_z is a vector of weights that defines the gray level parameters.

B. ASM-based Segmentation

Given a candidate test image, ASM-based segmentation has two main steps: initial contour estimate based on PDM and control points evolution for accurate segmentation. A

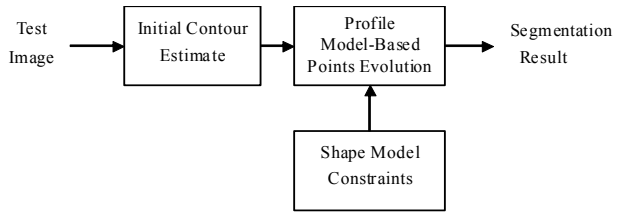

Fig. 1. Schematic of ASM-based Segmentation.

simplified schematic of this process is shown in Fig.1.

1) Initial Contour Estimate

It can be done by manually adjusting the mean shape using a transformation T, where T is a function of rotation θ, scaling s, and translation (t_x, t_y). This user-guided pose initialization lets the initial contour approximately close to the lung field in the test image under the constraints of the training set.

2) Points Evolution

Typical ASM method for segmentation only exploits the control point's profile model based on local gradient feature. For example, in a test image, best matches are made from each control points' profile model using the target points along the

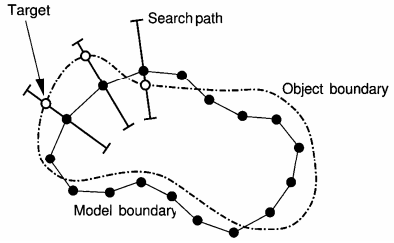

Fig.2. Searching an approximate model fit for target points to which control points may move [11].

searching profile (See Fig. 2). Then, a displacement of the model instance (dC) can be calculated according to the shape model, which leads to the corresponding adjustments to both the pose parameters ($d\theta$, ds, (dt_x, dt_y)) and shape parameters (db). This process is iterated until b converges or little change is seen along all control points.

C. GVF-ASM Segmentation

The schematic of the GVF-ASM method presented in [10] is shown in Fig. 3. The main differences from the typical ASM-based segmentation include an independent GVF

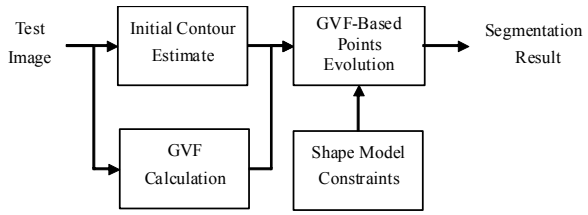

Fig. 3. Schematic of GVF-ASM method.

calculation and a GVF-driven points evolution.

1) GVF calculation

By introducing a global gradient vector flow field $g = (u(x,y), v(x,y))$ of a test image, the image's edge map f will be diffused so as to allow long range attraction of the contour towards the object boundary [9]. The vector field g is defined by minimizing the energy functional:

$$E_{ext} = \iint \eta(u_x^2 + u_y^2 + v_x^2 + v_y^2) + \left|\nabla f\right|^2 \left|g - \nabla f\right|^2 dxdy \quad (4)$$

where η is the smoothing factor, and ∇f is the gradient of the edge map. The u and v can be calculated by applying variational calculus and numeric methods (see details in [9]). It can be seen that target contour has large g value and on both sides of an edge the vectors point toward the edge.

2) Points Evolution

To integrate GVF with ASM, the control points of an active shape should be steered by both the direction and magnitude of g. Let $C=\left\{(x_1,y_1),(x_2,y_2),...(x_N,y_N)\right\}$ denote the current coordinates of the control points, and $C' = \left\{(x_1',y_1'),(x_2',y_2'),...(x_N',y_N')\right\}$ denote the coordinates of the points in the previous iteration. The points evolution equation including a given step size w and an annealing factor k is given as follows [10]:

$$C = C' + w \cdot k \cdot g(C') = C' + w\frac{p}{t^q} g(C'). \quad (5)$$

Note that the annealing factor $k = \frac{p}{t^q}$ (constants p, $q \geq 1$) decreases as the iteration time t increases.

III. PROPOSED METHOD

The GVF-ASM is an efficient technique for image segmentation, and has the potential to perform well for lung field segmentation. However, points evolution Eq. (5) has two

limitations: First, three parameters w, p and q need to be chosen before searching and may need to be adjusted every time for segmenting different test images; Next, in the application of segmenting lung field, the edges of lung contour in a chest radiograph are usually blurred, which means the magnitudes of the gradient vectors close to these contour edges changes smoothly. But in Eq. (5) the power function $1/t^q$ decreases too fast compared to the corresponding increase of magnitude of the gradient vector, which will lead to an early convergence.

In order to reduce the complexity and improve the accuracy of searching, we propose a new points evolution equation as follows:

$$C = C' + w \cdot \mathrm{sgn}(g(C')) \cdot e^{-|g(C')|} \quad (6)$$

where sign function *sgn* keeps the GVF vector's direction and the function *exp(-|g(C')|)* works as a smooth monotonically decreasing function which attracts the points to strong edges.

Fig. 4 illustrates the differences in the points evolution using Eqs. (5) and (6) for a given 1-D GVF $g = \{0.01, 0.02, ..., 1, -1, -0.99, ..., -0.01\}$. Note that g is a GVF field corresponding to 200 points ($1 \le x \le 200$), and the strong edges lie at $x = 100$ (when $g = 1$) and $x = 101$ (when $g = -1$). The horizontal axes represent the iteration time t, and the vertical axes represent the control point's new coordinate x at different t. In Fig. 4, the plots show the evolution of control point x over time t. It is observed in Fig. 4 (a) that evolution corresponding to both Eq. (5) and (6) converge to the expected strong edges ($x = 100$ and $x = 101$) with parameters $w = p = q = 1$ for Eq. (5) and $w = 1$ for Eq. (6). However, in Fig. 4 (b), the evolution of control point using Eq. (5) leads to an early false edge convergence with $w = q = 2$, $p = 1$, while the result of using Eq. (6) still

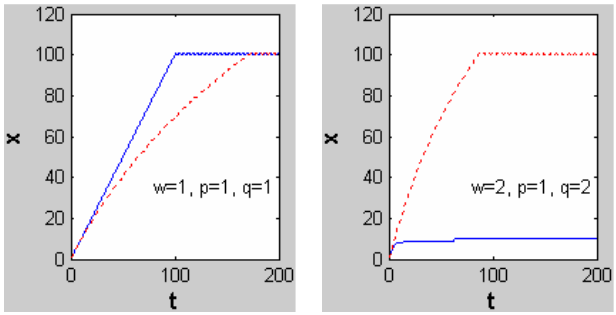

(a) (b)

Fig. 4. Example of 1-D point evolution using Eq. (5) and (6), where solid line (blue) for Eq. (5) and dotted line (red) for Eq. (6).

accurate with $w = 2$. In other words, points evolution Eq. (5) is sensitive to parameters selection.

Fig. 5 shows another example with a different 1-D GVF whose value changes more rapidly compared to the g considered in Fig. 4, $g = \{0.01, 0.06, ..., 0.96, -0.96, -0.91, ..., -0.01\}$, where the strong edges lie at $x = 20$ (when $g = 0.96$) and $x = 21$ (when $g = -0.96$). It is observed that the point evolution using Eq. (5) has strong ringing effect, and jumps too far away from the strong edges position.

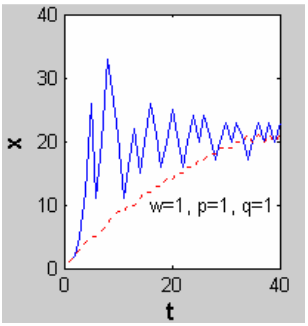

Fig. 5. Another example of 1-D point evolution using Eq. (5) and (6), where solid line (blue) for Eq. (5) and dotted line (red) for Eq. (6).

From the analysis of Fig. 4 and 5, the proposed points evolution equation works more accurate and stable, and it can also be proved in 2-D domain. Fig. 6 shows some intermediate

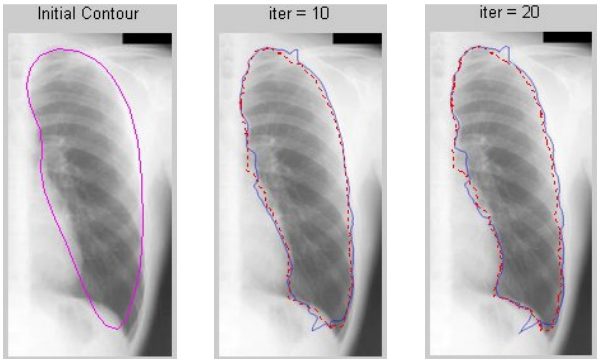

Fig. 6. 2-D points evolution using Eq. (5) and (6) with w=1, p=20, q=1, where solid line (blue) for Eq. (5) and dotted line (red) for Eq. (6).

results of our points evolution process compared to Eq. (5).

After the subsequent location for all control points are found, the shape model's parameters are updated within constraints. And the stopping criteria could be the number of iteration times or a threshold of the points' Euclidean distance between two consecutive iterations.

IV. Performance Evaluation

In this section, we present the performance evaluation of the proposed method, and compare it with the typical ASM [8] and GVF-ASM [10] methods.

For the evaluation we use two databases of Postero-Anterior chest radiographs: 1) The Japanese Society of Radiological Technology (JSRT) database; 2) CXR image database from the Univ. of Alberta Hospital. Images are resampled into 512×512 pixels (or close to this size) with 8 bit gray levels and are equally divided into left lung and right lung images. We define lung field as those parts of a chest radiograph which contain lungs not obscured by diaphragm, mediastinum and heart [12], before doing the experiments.

For images from JSRT database, we use an aligned training set of M = 20 left or right lung field contours, annotated with N = 30 control points. Six principal component vectors, which represent 90% of the total variance of the training set, are used

to model the shape variation of the aligned training set of the lung field. Similarly, for our CXR database with fewer chest radiographs, M = 10, N = 30. After PDM-based rough contour initialization on the test image, segmentation methods of typical ASM, GVF-ASM and the proposed method are performed. 10 normal chest radiographs from JSRT database and 10 abnormal from CXR database are tested. Fig. 7 shows

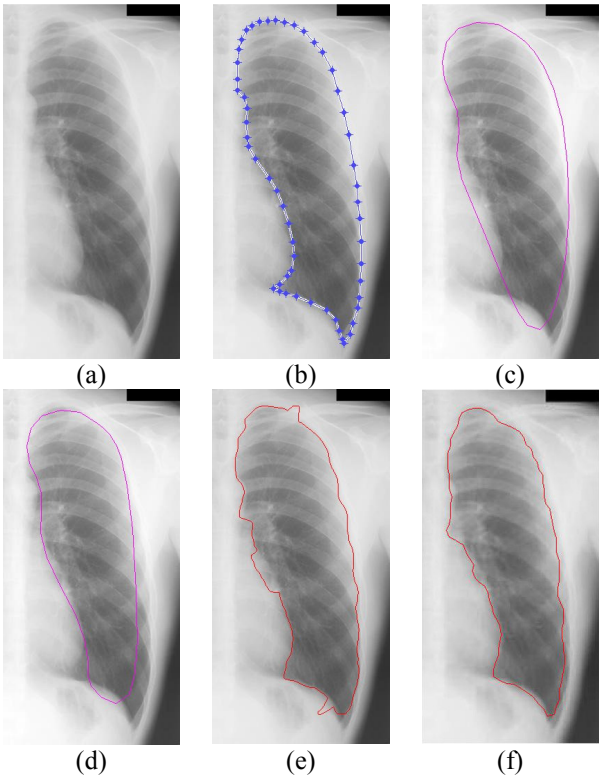

Fig.7. Performance of the proposed method for lung field segmentation (a) Left lung image for test; (b) Manually outlined contour; (c) A PDM-based initialization using 20 training images; (d) ASM [8] result; (e) GVF-ASM [10] result; (f) Proposed method's result.

example images of one experiment.

Expert radiologists helped to manually draw lung field contours for both test and training images using a display program with a mouse-controlled interface. Assuming the manually outlined contour as the ground truth, the performances of different segmentation methods are evaluated by the overlapping degree Ω between manually outlined contour A and contour B obtained by using semi-automatic segmentation methods. In this paper we use Ω as the performance measure of a segmentation technique, and Ω is computed as follows:

$$\Omega = \frac{\mathbf{A} \cap \mathbf{B}}{\mathbf{A} \cup \mathbf{B}} = \frac{\mathrm{TP}}{\mathrm{TP+FP+FN}} \times 100\% \qquad (7)$$

where **A** and **B** are the sets of all pixels enclosed by contours A and B. And TP, FP, FN stand for the true positive, false positive and true negative areas, respectively. The evaluation results are listed in TABLE I, where μ, σ, and median are the expected value, standard deviation and median value of Ω, respectively. It can be seen that our method outperforms the other algorithms by at least 3-5% considering both mean and median.

TABLE I
SEGMENTATION METHODS EVALUATION

JSRT Database	Left Lung			Right Lung		
	μ	σ	median	μ	σ	median
ASM[8]	83.4 %	4.6 %	84.2%	84.1 %	3.3 %	85.2%
GVF-ASM[10]	84.9 %	3.3 %	84.6%	87.8 %	3.0 %	87.4%
Proposed	88.1 %	2.7 %	88.6%	90.1 %	2.7 %	89.6%
CXR Database	Left Lung			Right Lung		
	μ	σ	median	μ	σ	median
ASM[8]	77.4 %	6.8 %	77.1%	84.6 %	4.5 %	84.7%
GVF-ASM[10]	80,8 %	6.7 %	82.5%	87.6 %	2.1 %	87.2%
Proposed	83.8 %	7.6 %	84.7%	89.3 %	2.1 %	89.0%

V. CONCLUSIONS

We proposed a GVF-ASM method with exponential points evolution for lung field segmentation. The experimental results demonstrated that the proposed method improves the robustness and accuracy of the segmentation.

REFERENCES

[1] B. V. Ginneken, B. M. T. H. Romeny, and M. Viergever, "Computer-aided diagnosis in chest radiography: a survey," IEEE Trans. Med. Imaging, vol 20 (12), pp. 1228–1241, 2001.

[2] S. G. Armato III, M. L. Giger, and H. MacMahon, "Automated lung segmentation in digitized posteroanterior chest radiographs," Acad. Radiol., vol 5, pp. 245–255, 1998.

[3] X. Xu and K. Doi, "Image feature analysis for computer-aided diagnosis: Detection of right and left hemidiaphragm edges and deliniation of lung field in chest radiographs," Med. Phys., vol. 23, pp. 1613–1624, 1996.

[4] F. M. Carrascal et al., "Automatic calculation of total lung capacity from automatically traced lung boundaries in postero-anterior and lateral digital chest radiographs," Med. Phys., vol. 25, pp. 1118–1131, 1998.

[5] T. Yu, J. Luo, A. Singhal and N. Ahuja, "Shape regularized active contour based on dynamic programming for anatomical structure segmentation," Proc. of SPIE Medical Imaging, pp. 419–430. 2005.

[6] B. V. Ginneken et al, "Active shape model segmentation with optimal features," IEEE Trans. Med. Imag., vol. 21 (8), pp. 924–933, 2002.

[7] M. Kass et al, "Snakes - Active Contour Models," International Journal of Computer Vision, vol. 1(4), pp. 321–331, 1987.

[8] T. F. Cootes et al, "Active shape models: their training and application," CVIU, vol. 61 (1), pp. 38–59, 1995.

[9] C. Xu and J. L. Prince, "Snakes, shapes, and gradient vector flow," IEEE Trans. on Image Proc., pp. 359–369, 1998.

[10] X. Yuan, B. Giritharan, J. Oh, "Gradient vector flow driven active shape for image segmentation," Proc. of International Conference on Multimedia & Expo., pp. 2058–2061, 2007.

[11] M. Sonka, V. Hlavac, R. Boyle, *Image Processing, Analysis, and Machine Vision*, Toronto: Thomson Learning, 2008, pp. 461.

[12] B. V. Ginneken, "Computer-aided diagnosis in chest radiographs," P.h.D. dissertation, Utrecht Univ., Utrecht, The Nederlands, 2001.